

This is a non-peer reviewed pre-print submitted to EarthArXiv.

# Machine Learning Reveals the State of Intermittent Frictional Dynamics in a Sheared Granular Fault

## Authors:

C. X. Ren<sup>1†\*</sup>, O. Dorostkar<sup>2†\*</sup>,

B. Rouet-Leduc<sup>1</sup>, C. Hulbert<sup>1</sup>, D. Strebel<sup>3</sup>, R. A. Guyer<sup>1</sup>, P. A. Johnson<sup>1</sup>, J. Carmeliet<sup>2</sup>

<sup>1</sup> Geophysics Group, Los Alamos National Laboratory, MS D446, Los Alamos, New Mexico 87545, USA

<sup>2</sup> Department of Mechanical and Process Engineering, Swiss Federal Institute of Technology Zürich (ETH Zürich), Tannenstrasse 3, CH-8006 Zürich, Switzerland

<sup>3</sup> Swiss Federal Laboratories for Materials Science and Technology (Empa), Überlandstrasse 129, CH-8600 Dübendorf, Switzerland

†Equal contribution

\*Corresponding authors:

Omid Dorostkar (Email: [domid@ethz.ch](mailto:domid@ethz.ch)) (ID: [orcid.org/0000-0002-7758-4919](https://orcid.org/0000-0002-7758-4919))

Christopher. X. Ren (Email: [cren@lanl.gov](mailto:cren@lanl.gov)) (ID: [orcid.org/0000-0002-0787-6713](https://orcid.org/0000-0002-0787-6713))

## **Abstract**

The seismogenic plate boundaries are presumed to behave similar to densely packed granular medium, where fault and blocks systems rapidly rearrange the distribution of forces within themselves, as particles do in slowly sheared granular systems. We use machine learning and show that statistical features of velocity signals from individual particles in a simulated sheared granular fault contain information regarding the instantaneous global state of intermittent frictional stick-slip dynamics. We demonstrate that combining features built from the signals of more particles can improve the accuracy of the global model, and discuss the physical basis behind decrease in error. We show that the statistical features such as median and higher moments of the signals that represent the particle displacement in the direction of shearing are among the best predictive features. Our work provides novel insights into the applications of machine learning in studying frictional processes that take place in geophysical systems.

## **Keywords**

Machine learning, fault mechanics, granular materials, DEM, friction, stick-slip

## 1 Introduction

Characterizing the state of friction in granular flows in Earth can significantly improve our understanding of geological and geophysical frictional processes that take place in earthquakes, landslides, avalanches, debris flows and soil liquefaction [van der Elst et al., 2012; Brzinski & Daniels, 2018; Rouet-Leduc et al., 2018]. In a critical loading configuration, sheared granular layers can exhibit stick-slip dynamics that resemble the intermittent dynamics of earthquakes [Brace & Byerlee, 1966, 1970; Johnson et al., 1973; Scholz, 1998]: during the stick phase, which is the earthquake nucleation phase, the elastic strain energy builds up and at slip, the energy is released as an earthquake [Dorostkar & Carmeliet, 2018].

Sheared granular systems can be considered analogous to the macroscopic dynamics of faults in Earth [Anderson, 2007], where both systems exhibit intermittent dynamics: motion at boundaries results from the differential motion of the particles or juxtaposed tectonic blocks; the release of energy is due to rearrangement of particles, in sheared granular layers or earthquakes in fault zones [Meroz & Meade, 2017]. The statistical distributions of slip events in both laboratory and numerical fault gouge are shown to follow the Gutenberg-Richter law, providing similar  $b$ -values [Gutenberg & Richter, 1944; Dahmen et al., 2011; Uhl et al., 2015; Dorostkar, 2018; Rivière et al., 2018]. The analysis of fluctuations in Global Positioning System (GPS) observations of inter-seismic motion from the southern California plate boundary has identified the same statistical distribution of velocity fluctuations as in slowly sheared granular media [Meroz & Meade, 2017]. This may suggest that the plate boundary can be understood as a densely packed granular medium, predicting a characteristic tectonic length scale and relating the characteristic duration and recurrence interval of earthquakes [Meroz & Meade, 2017].

Numerical tools such as Discrete Element Method (DEM) simulations are a useful means to shed light on the frictional processes that govern fault slip [Dorostkar, Johnson, et al., 2017; Dorostkar et al., 2018]. Numerical simulations can provide micro-scale information [Dorostkar, Guyer, et al., 2017] whilst most experimental studies of stick-slip dynamics are opaque. Further, assessing the internal stress state of a granular system is notoriously difficult, and even photo-elastic, optical, and tomographic techniques require specialized materials or slow scanning times [Brzinski & Daniels, 2018]. DEM simulations can provide insight into the inner workings of such systems clarifying the complexities of frictional behaviour. Furthermore, DEM modelling enables us to extract the information needed to build models for characterizing the frictional state of a fault system subject to shear.

The recent applications of machine learning in earthquake identification [Perol et al., 2018; Ross et al., 2018], association for seismic arrivals [McBrearty et al., 2019], estimation of fault displacement rate in the Cascadia subduction zone [Rouet-Leduc et al., 2019], detection of similarities between slow and fast slip events [Hulbert et al., 2019] and prediction of remaining time to failure [Rouet-Leduc et al., 2017; Corbi et al., 2019] are promising developments underscoring the rich potential of modern data analysis techniques. Machine learning techniques can help us to better understand and address complex open questions in geoscience, since they can augment our intuition and help to reveal structure in high-dimensional datasets [Kong et al., 2018; Ross et al., 2019].

Capitalizing on the advantages of DEM simulations and machine learning techniques, here we use a distributed gradient boosting algorithm [J. Friedman et al., 2000; J. H. Friedman, 2002; Chen & Guestrin, 2016] to build models that are able to estimate the highly irregular frictional

state in a sheared granular media. By using the velocity signals of individual flagged particles inside the granular fault, the Extreme Gradient Boosting (XGBoost) model in this paper shows that the individual grains contain predictive information concerning the global frictional state during a stick-slip cycle. We posit that based on the statistical similarities between our numerical simulations, laboratory experiments and plate boundary scale GPS velocity fluctuations [Meroz & Meade, 2017; Rouet-Leduc et al., 2019], the granular approximation in numerical simulations provides a useful mathematical framework for understanding and characterizing the frictional processes that take place in a tectonic plate boundary [Meroz & Meade, 2017]. Our developments and findings in this paper provide novel insights into the dynamics of sheared granular systems, which we believe open promising windows for future applications of machine learning in studying frictional processes that take place in geophysical systems.

## 2 Materials and Methods

Figure 1a illustrates the DEM granular layer with size of  $11 \times 1.5 \times 0.8 \text{ mm}^3$  containing 7996 spherical particles with a uniform, poly-disperse particle size distribution ranging 90-150  $\mu\text{m}$ . On the sample top and bottom, we use two corrugated plates with high surface roughness modelled by a friction coefficient of 0.9 between the plates and particles to totally engage the fault blocks with granular particles (see Fig.1a insets). The position of the upper corrugated plate is adapted continuously to maintain constant the confining stress. A displacement-controlled servomechanism moves the bottom corrugated plate along the x direction at constant velocity of 600  $\mu\text{m/s}$ . The confining stress is 10 MPa. On the front- and back-side of the sample, we employ frictionless walls with the same elastic properties as the particles to avoid rigid wall boundary conditions. Periodic boundary conditions are applied at the left and right sidewalls in x direction. The particle density is 2900  $\text{kg/m}^3$ , which results in a DEM time step of  $15 \times 10^{-9}$  seconds. The granular flow remains in the quasi-static regime by setting the inertial number to be below  $10^{-3}$  [MiDi, 2004]. We use LIGGGHTS [Goniva et al., 2012; Kloss et al., 2012] to model the granular system. The properties of DEM model is fully presented in Table 1 of Supplementary Information.

We test for the relationship between the instantaneous global frictional state of the simulated system and the particle velocity by applying a supervised learning approach. We calculate statistical features of the particle velocity signal for short moving time windows, as described in [Rouet-Leduc et al., 2017]. These pre-determined features consist of various higher-order statistical moments, percentiles, and inter-quartile ranges within the windows. The machine learning (ML) model utilizes these features in order to estimate the instantaneous, global friction coefficient of the system for the final step of a time window for which the features are extracted. The time windows considered in this work consist of 10 time steps from the DEM simulation, equal to  $15 \times 10^{-8}$  seconds, and overlap each other by 9 time steps. Finally, we smooth the features across 30 time steps to achieve the best results.

We utilize the XGBoost implementation [Chen & Guestrin, 2016] of an ML algorithm known as gradient boosted decision trees [J. H. Friedman, 2002], an ensemble method for decision trees [Breiman, 1984], with an L2 loss function (minimizing mean squared error). We choose L2 over L1 as a loss function, as in this case we are looking to capture the behavior of the slip events, which can be considered ‘outliers’ in the overall distribution of the macroscopic friction values of the system. Boosting is a strategy whereby multiple ‘weak’ models are sequentially combined into a ‘strong’ composite model by fitting each new weak learner to the residuals of the previous iteration (see Supplementary Information).

The training set for this model comprises the first 80% of the simulated data and the testing set used to evaluate the performance of the model consists of the remaining 20%. We train the gradient boosting model by providing the features derived from the sliding time windows as input, and the macroscopic friction calculated from the DEM simulations as label. We then test the trained model on the testing set, by providing only the features of the velocity signal from a single particle attempting to estimate the unseen friction of the system during this period. The performance of our model is then evaluated with respect to the test ground truth (macroscopic friction calculated from the DEM simulations as label) using the coefficient of determination as an evaluation metric.

In order to evaluate the relative importance of features, we utilize Shapely Additive Explanations (SHAP) values, a relatively novel method of attributing feature importance based on game theory [S. M. Lundberg & Su-In Lee, 2017]. Traditionally, global feature importance for decision tree algorithms are calculated using gain, split count, or permutation methods [Auret & Aldrich, 2011]. However, it has been shown that feature importance values calculated in the aforementioned manners are inconsistent: the mechanics of a model can change such that it relies more on a given feature to make predictions, yet the importance estimate of said feature can decrease [Lundberg et al., 2018]. SHAP values combine Shapley values from game theory [Shapley, 1953] with the conditional expectation function of the model. Given a subset of input features, the features are modeled as ‘players’ in a co-operative game where the end goal is prediction. The ‘pay-outs’ from the game are thus the feature importance, and calculated by determining the contribution of each ‘player’ to the game [S. M. Lundberg & Su-In Lee, 2017] (See Supplementary Information for more details).

### 3 Results

For training process, the feature space is constructed for 4 properties of the particles i.e. the x, y and z-components of particle velocity (denoted in this work as  $V_x$ ,  $V_y$  and  $V_z$ ) together with its magnitude,  $V$ . Fig. 2a shows the time series of macroscopic friction and  $V_x$  for particle 2146 on the right-hand y-axis. We observe continuous fluctuations during the stick phase and rapid bursts in particle velocity associated with each slip event. After the training of the ML model (Fig. 2b), the velocity signal of particle id 2146 exhibits the best performance among all of the particles in the system with a model performance of  $R^2 = 0.57$  in Fig. 2c. The  $R^2$  is calculated for the gradient boosting model trained on statistical features from the velocity signal of a single particle using the process described in Sec. 2. This observation shows that a single particle can be used to determine the macroscopic friction of the entire system it belongs to: the statistical characteristics of its velocity signal are a fingerprint of the global frictional state.

We perform the ML analysis for the velocity signals of all particles in the fault model; Fig. 3a shows the distribution of  $R^2$  scores for 7996 particles during the testing period. The median of this distribution is  $R^2 = 0.09$ , with a 90<sup>th</sup> percentile value of  $R^2 = 0.3$ , indicating that a large number of particles carry limited useful information concerning the macroscopic frictional state of the system over the testing period. We posit that since a single particle is not involved in the entire structure of granular contacts, and that some of the slip events may be localized in a relatively small region of the system, the particle may not be sensitive to rearrangements far away from its position.

We also study the feature importance in our ML model that is developed from the velocity signal of a single particle. Figure 3b shows the ten most important features for the ML model

giving the results shown in Fig. 2. The feature importance is expressed in terms of mean absolute SHAP values, as detailed in Sec. 2. The impact of each individual instance of the features at each row is shown on the x-axis. We note that two complementary features display the largest range of SHAP values: the median value of  $V_x$ , and the 4<sup>th</sup> moment of  $V$ . These two features are complementary in terms of their statistical properties: the median of a distribution is robust to outliers, whereas the 4<sup>th</sup> moment is in fact a measure of ‘heaviness’ of the tail of a distribution, and is extremely sensitive to outliers [Đorić et al., 2009]. We remark that these two most important features are followed narrowly by the 4<sup>th</sup> moment of  $V_y$  (Fig. 3b), indicating that slip events are not sensed by the particle only in the shearing direction, but also in the direction of system compaction at slip [Dorostkar & Carmeliet, 2019]. Interestingly, a moving median provides a robust estimate of the trend of a time series when variations from the trend are Laplace distributed [Arce, 2005], as is the case with the velocity of the particle. The features deemed important by the model can thus be interpreted as the underlying trend of the velocity (or energy) of the particle, as well as an ‘event detector’ defined by the 4<sup>th</sup> moment of the velocity. The relationship between the underlying trend of the particle energy and the macroscopic friction of the system is in good agreement with the results reported in laboratory by Rouet-Leduc *et al.* [2018], where the key feature for the estimation of fault friction is the variance of the acoustic signal, which is directly related to the seismic energy contained in a given time window.

Figure 3c shows a SHAP dependence plot, similar in nature to partial dependence plots often used for the interpretation of ML models [Greenwell, 2017]. The feature instances are colored by the values of another feature (in this case, the median of  $V_x$ ) to reveal potential feature interactions. Here we show the logarithm of the 4<sup>th</sup> moment of x-component of the particle velocity, plotted against SHAP value, or ‘importance’ as discussed in Sec. 2. This feature clearly dominates the model estimations as it approaches large values, corresponding to larger slip events, as shown in Fig. 3f, where sudden increases in the 4<sup>th</sup> moment (green trace) align with large drops in the macroscopic friction, confirming that the 4<sup>th</sup> moment of the particle velocity operates as an event detector in our model

Figure 3d shows the SHAP dependence plot for the median of  $V_x$ , colored by the logarithm of the 4<sup>th</sup> moment. We observe two regimes where the median has an impact on the ML model: one where the value of the 4<sup>th</sup> moment is large (approximately  $>10^{-1}$ ), and one where it is far smaller ( $\sim 7$  orders of magnitude). We speculate this interaction exists due to the fact that large slip events can induce changes in the underlying trend of the velocity of the particle. This is shown in Fig. 3e where the median (red trace) correlates with small variations in the friction between the larger slip events, but also decreases gradually across these events, which are sensed by the 4<sup>th</sup> moment of the velocity.

We demonstrate that the performance of the ML model can be improved by combining the features used for the single particle mode with features derived from the velocity of a different particle. Figure 4a shows the improved model (black trace) plotted against the best single particle model (red trace) and ground truth (blue trace). Although the model does not always estimate a more accurate value for the macroscopic friction across the test set, the improvements made by including the features from the second particle are substantial: the test  $R^2$  of the model improves to a value of 0.7. In particular, we note the model error is vastly reduced towards the end of the test set, in the time steps ranging between  $3.3\text{-}3.5 \times 10^8$ , where the 4<sup>th</sup> moment of the combined particle exhibits more spikes, corresponding to the response of the particle to slip events occurring in the system, as is shown in Fig. 4b. The increase in performance of the ML model shows that

recording the velocity signals in more regions of the fault system may help to estimate the state of friction more accurately. Adding more particles in the preparation of the feature space does not necessarily improve the performance of the model as the model requires a consistent mapping between the training and testing sets.

In Fig. 4c, we show the change in distribution of test  $R^2$  scores between the single best particle (ID=2146, shown in red), and the features from this particle (ID = 2146) combined with features built from all other particles in the simulation (black). We hypothesize that the ML model improves as it has access to more information concerning the state of the system, but through the similar features as for the single particle. This fact is evidenced in Fig. 4d, which shows that the top ten most important features for the combined ML model mainly consists of the skewness measures, as well as features consisting of the moving median, which are similar to those found for the single particle, shown in Fig. 3b. Interestingly, of the 7995 particles shown in the combined distribution in Fig. 4c (black), only 189 combinations (approximately 2%) improve the test  $R^2$  beyond that of the model built using only features from particle 2146. Based on these results we can conclude that not only can the instantaneous global state of the simulated system be recovered from the characteristics of a single particle in this system, but that this particle is ‘privileged’ in terms of the information it has access to, as only 2% of the particles provide complementary information when added to the model. We speculate that this ‘privileged’ position is likely due to the relative position of the particle and the force network through the system: the particle must be somewhat free to move in order to transmit information concerning global state of the system, but also close enough to areas of change in the force network to avoid uninformative ‘rattling’ behavior. This extremely interesting observation with regards to the information content of the bead pack is something beyond the scope of this letter but will be the subject of future investigations.

#### 4 Summary and Conclusions

We simulate a sheared granular layer and use machine learning to estimate the instantaneous, bulk friction of system. We show that the velocities of individual particles contain predictive information regarding the global state of the system. We also show that combining signals of more particles can improve our models’ ability to capture the evolution of frictional state of the system. Our analyses show that the statistical features i.e. median and higher moments of signals that represent the particle displacement in the direction of shearing during the stick phase and the particle displacement magnitude at slip event are among the best estimators of the friction of the system.

The fact that only some particles in the system offer instantaneous predictability of the friction is fascinating and demonstrates not all grain velocities are equal in their information content. This may be due to non-stationarity in the simulation, as the training set may not fully contain informative velocity behavior for modelling the testing set. When analyzing the bulk velocity, there may be cancellation effects of the ensemble that diminish instantaneous predictability. We have observed that the most predictive grains are located near regions of high stress force chains, but not in them. The predictive grains are also not ‘rattlers’. The relative contributions of different particles in the ensemble and why contributions are markedly different is a large undertaking and will be addressed in future works.

In field scale, the observations of diverse fault activity is suggested to be explained by a model where plate boundaries are considered as macroscopic granular shear zones near the

jamming transition [Ben-Zion, 2008] with effective particle sizes bigger than 10 km enabling earthquakes themselves to redistribute forces within plate boundaries by rearranging force chains [Meroz & Meade, 2017]. Our work shows the potential of numerical methods and in particular, the discrete element approach to improve the understanding of frictional processes that dictate fault frictional slip. This letter also highlights the ability of ML algorithms to characterize the highly irregular frictional behavior of a fault system and identify signals and parameters of importance to the modelling of such systems.

### **Acknowledgments**

OD and JC thank ETH Zürich for funding and Empa for infrastructural support. CR, BRL, CH, PJ and RG acknowledge institutional support (LDRD) at Los Alamos for funding. The data related to this paper can be obtained by contacting the corresponding authors at [domid@ethz.ch](mailto:domid@ethz.ch) or [cren@lanl.gov](mailto:cren@lanl.gov).

## Figures

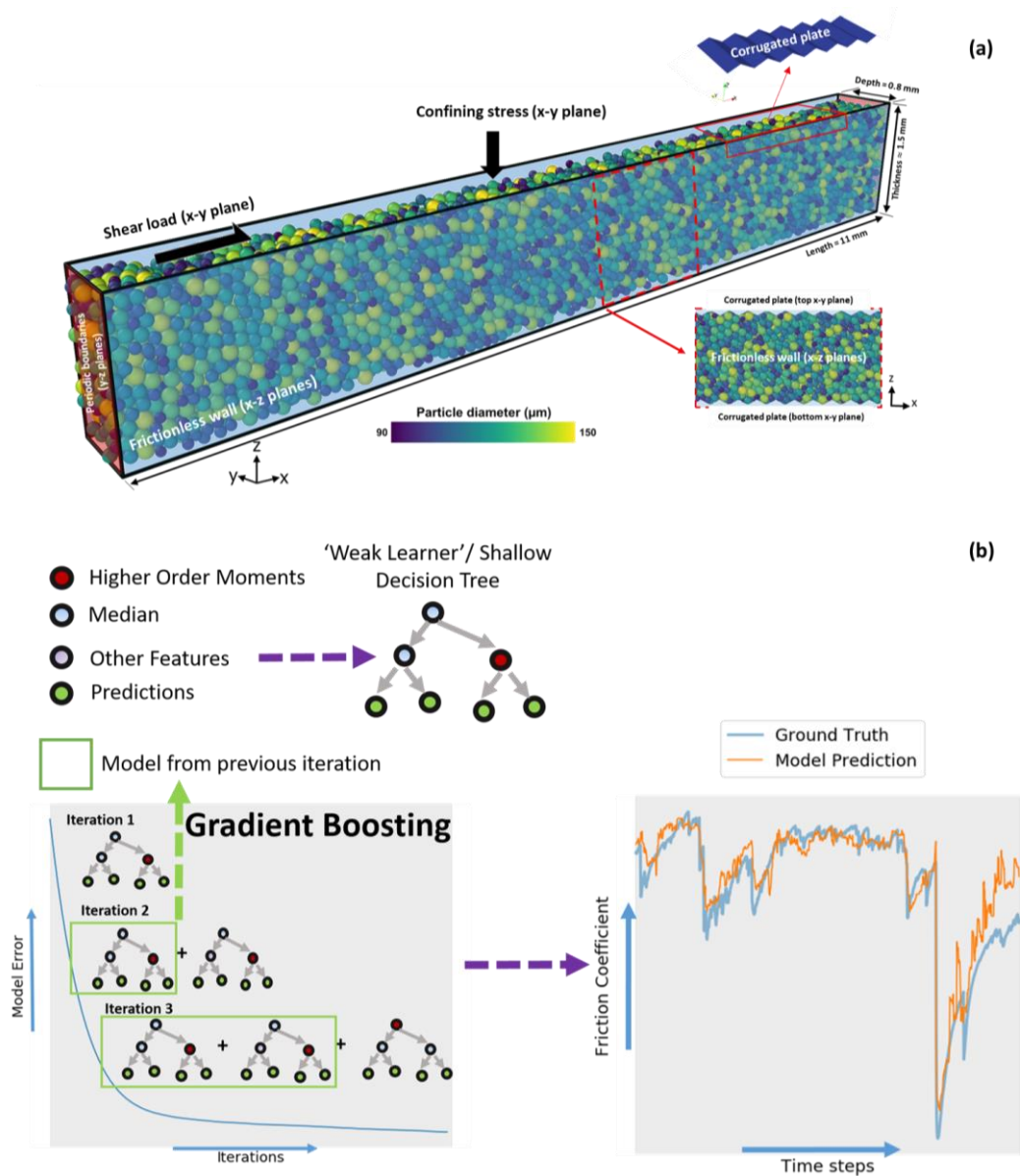


**Figure 1:** (a) Granular fault model with poly-disperse particle diameter distribution of 90-150 micrometer. The fault system is confined in z-direction and sheared in x-direction. Periodic boundary conditions are employed on y-z planes. The shear load is applied along the x-y plane, where two corrugated plates are used on top and bottom x-y planes of the gouge simulating a rough fault surface. (b) A simplified diagram of the gradient boosting process. At each iteration, a weak learner is fit to the residuals from the previous iteration, and is added to the overall model. The model at each iteration is thus an ensemble of the weak learners from previous iterations with an additional weak learner fit to the residuals of the previous ensemble. This iterative process results in the increasing predictive ability of the model, and the reduction of training error.

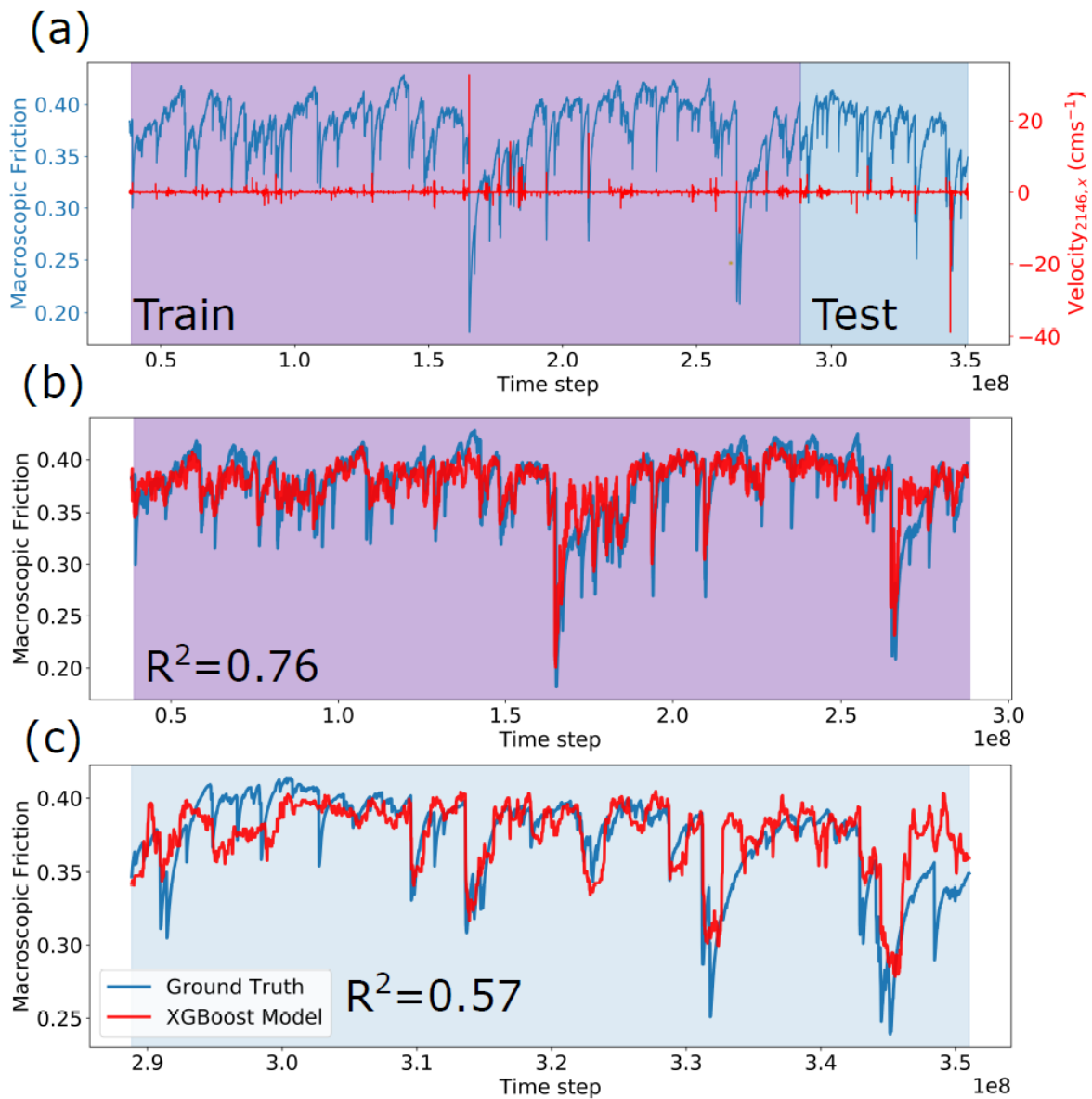


**Figure 2.** XGBoost estimates the instantaneous frictional state of the DEM system from the velocity signal of a single particle. (a) Frictional state of the system (blue curve) throughout the simulation, the violet and blue shaded regions correspond to the training and test labels (target output) respectively. The velocity signal for a single particle is shown in red, this is the raw data stream used to construct features. (b) Performance of the XGBoost model (in red) vs the ground truth (blue) for the training set. (c) Performance of the model for the testing set with a performance of  $R^2=0.57$ .

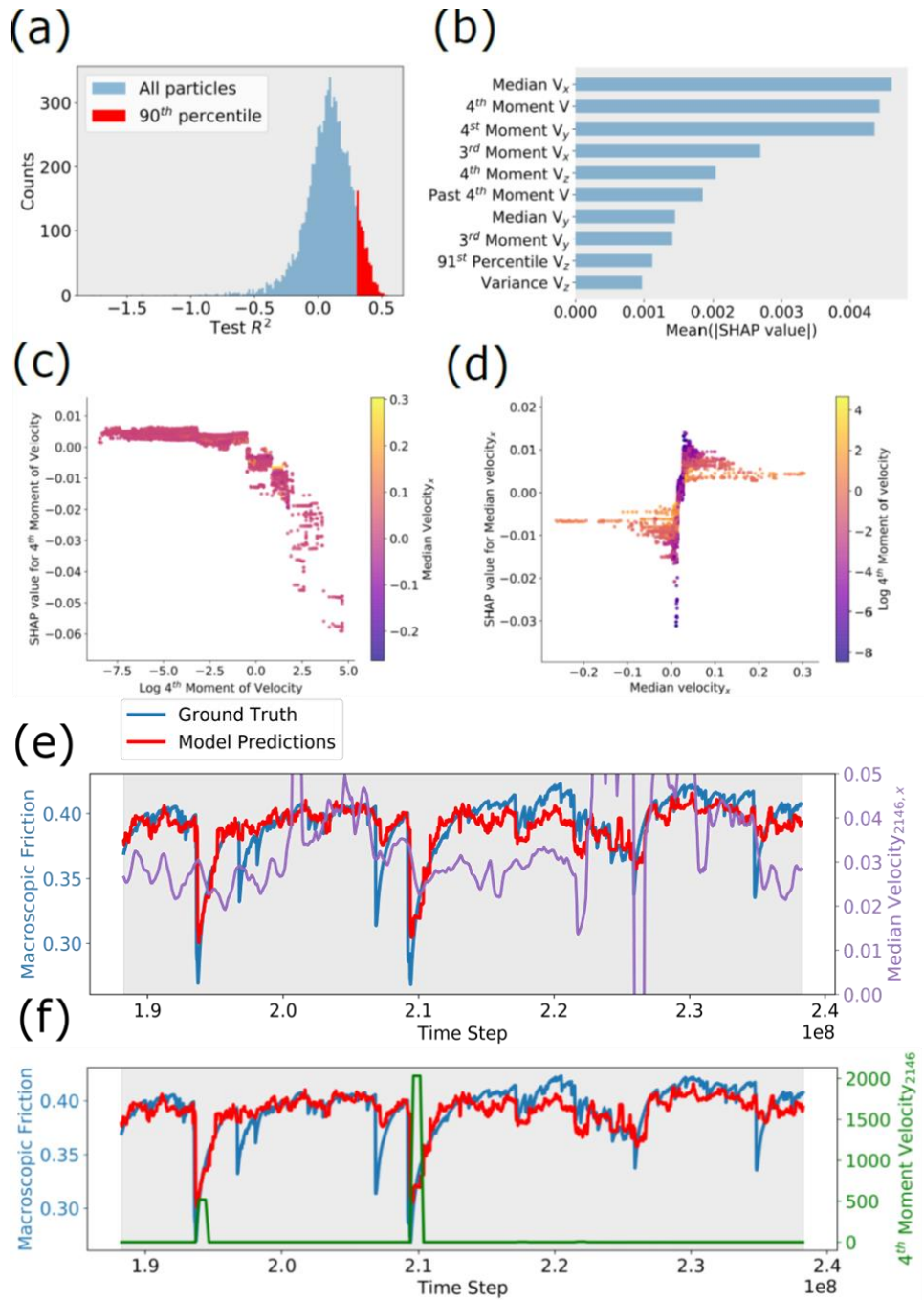


**Figure 3:** Model outputs: (a) Distribution of test  $R^2$  scores for XGBoost models trained on features built from the velocity signal of each particle in the simulation, with the 90<sup>th</sup> percentile of the scores highlighted in red (test  $R^2 \geq 0.3$ ). (b) Top 10 features for the model shown in Figure 2(b) based on mean absolute SHAP value, ordered from best to worst top down. (c) Dependence plot for the log 4<sup>th</sup> moment, colored by the median x-component feature. (d) SHAP dependence plot for the median value of the x-component colored by the log 4<sup>th</sup> moment of the velocity. (e-f) Feature vs model plots for the median x-component and the 4<sup>th</sup> moment of the velocity signal. The median values have been clipped between 0 and 0.5 for visualization purposes.

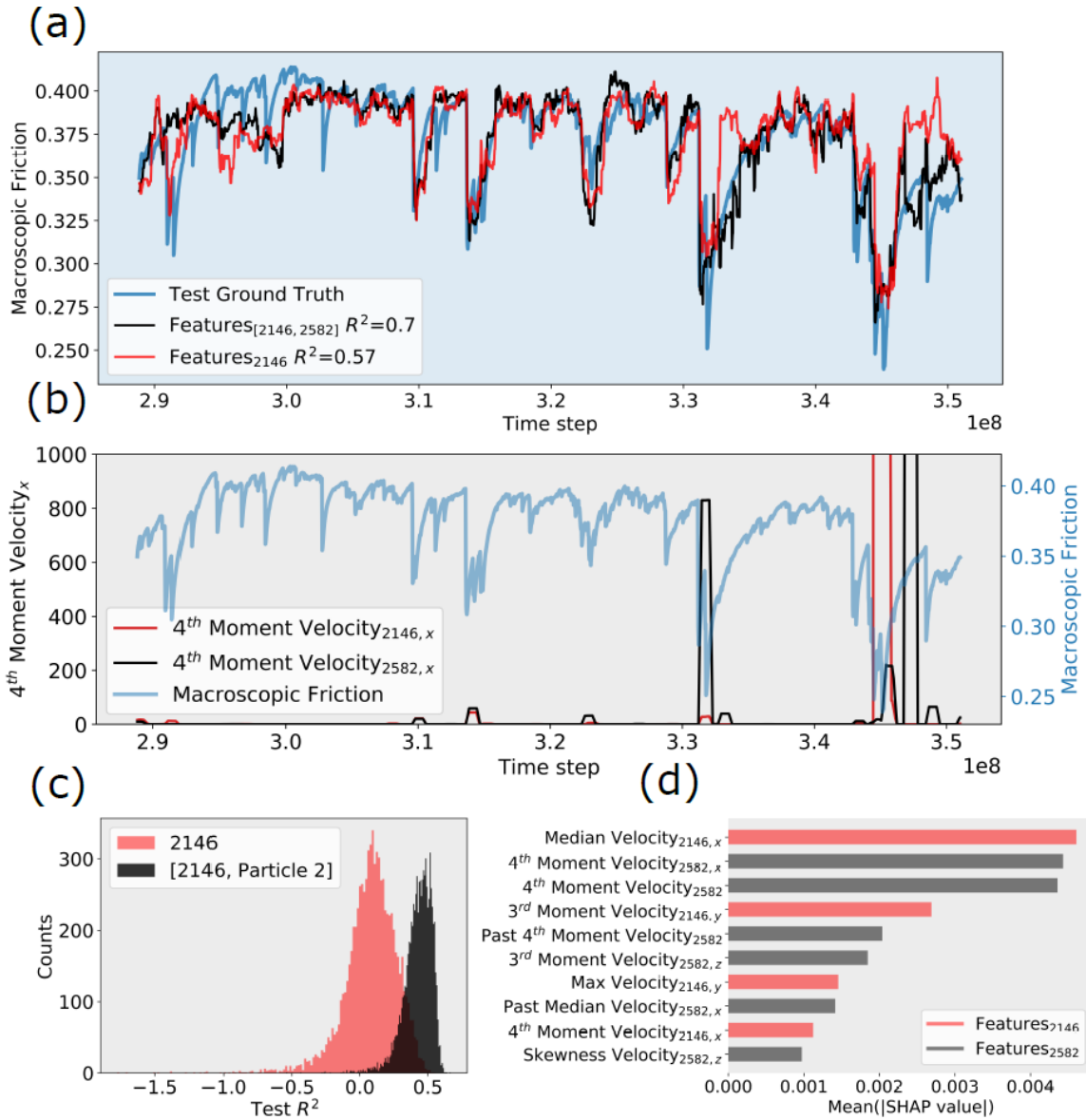


Figure 4: Results of ML model with combined features for two particles: (a) Improved model performance of (black trace,  $R^2=0.7$ ) of XGBoost model trained on features from particles ID 2146 and 2582, compared to using the features only from 2146 (red trace) (b) 4<sup>th</sup> Moment of the velocity from the two particles, 2146 in red and 2582 in black with the macroscopic friction in blue, we can see that the black trace includes more spikes in the 4<sup>th</sup> moment. (c) Shift in the distribution of test  $R^2$  for single particles (red bins), and all other particles combined with particle 2146 (black bins). (d) Top ten combined features for the model shown in (a).

## Supplementary Information

# Machine Learning Reveals the State of Intermittent Frictional Dynamics in a Sheared Granular Fault

### Authors:

C. X. Ren<sup>1†\*</sup>, O. Dorostkar<sup>2†\*</sup>,

B. Rouet-Leduc<sup>1</sup>, C. Hulbert<sup>1</sup>, D. Strebel<sup>3</sup>, R. A. Guyer<sup>1</sup>, P. A. Johnson<sup>1</sup>, J. Carmeliet<sup>2</sup>

<sup>1</sup> Geophysics Group, Los Alamos National Laboratory, MS D446, Los Alamos, New Mexico 87545, USA

<sup>2</sup> Department of Mechanical and Process Engineering, Swiss Federal Institute of Technology Zürich (ETH Zürich), Tannenstrasse 3, CH-8006 Zürich, Switzerland

<sup>3</sup> Swiss Federal Laboratories for Materials Science and Technology (Empa), Überlandstrasse 129, CH-8600 Dübendorf, Switzerland

†Equal contribution

\*Corresponding authors:

Omid Dorostkar (Email: [domid@ethz.ch](mailto:domid@ethz.ch)) (ID: [orcid.org/0000-0002-7758-4919](https://orcid.org/0000-0002-7758-4919))

Christopher. X. Ren (Email: [cren@lanl.gov](mailto:cren@lanl.gov)) (ID: [orcid.org/0000-0002-0787-6713](https://orcid.org/0000-0002-0787-6713))

## 1 DEM

In DEM, the equations of motion are solved for each particle:

$$\Sigma \mathbf{F}_p = \mathbf{m} \left( \frac{d}{dt} \mathbf{u}_p \right), \quad (1)$$

$$\Sigma \mathbf{T}_p = \mathbf{I} \left( \frac{d}{dt} \boldsymbol{\omega}_p \right), \quad (2)$$

where  $m$ ,  $I$ ,  $u_p$  and  $\omega_p$  are the mass, the moment of inertia and the translational and angular velocity of particle, and  $F_p$  and  $T_p$  are the forces and torques acting on particle, respectively. In soft sphere DEM, the particle-particle contact allows an overlap between them and the contact law is described by a combination of different rheological elements such as spring, dashpot and frictional slider [Dorostkar, 2018]. Using nonlinear Hertzian particle-particle contact law, the normal and tangential contact forces and the spring and damping coefficients are calculated as follow [Hertz, 1882; Di Renzo & Di Maio, 2004]:

$$\mathbf{F}_{pn} = -k_{pn} \delta \boldsymbol{\varepsilon}_{pn} + c_{pn} \delta \mathbf{u}_{pn}, \quad (3)$$

$$\mathbf{F}_{pt} = \min \left\{ \left| k_{pt} \int_{t_{c,0}}^t \delta \mathbf{u}_{pt} dt + c_{pt} \delta \mathbf{u}_{pt} \right|, \mu_c \mathbf{F}_{pn} \right\}, \quad (4)$$

$$k_{pn} = \frac{4}{3} Y^* \sqrt{R^* \delta \boldsymbol{\varepsilon}_{pn}}, \quad (5)$$

$$k_{pt} = 8 G^* \sqrt{R^* \delta \boldsymbol{\varepsilon}_{pn}}, \quad (6)$$

$$c_{pn} = -2 \sqrt{\frac{5}{6}} \times \frac{\ln(r)}{\sqrt{\ln^2(r) + \pi^2}} \times \sqrt{2 Y^* \sqrt{R^* \delta \boldsymbol{\varepsilon}_{pn}} m^*}, \quad (7)$$

$$c_{pt} = -2 \sqrt{\frac{5}{6}} \times \frac{\ln(r)}{\sqrt{\ln^2(r) + \pi^2}} \times \sqrt{8 G^* \sqrt{R^* \delta \boldsymbol{\varepsilon}_{pn}} m^*}, \quad (8)$$

where  $k_{pn}$  and  $k_{pt}$  are the normal and tangential spring stiffness,  $c_{pn}$  and  $c_{pt}$  are the normal and tangential damping coefficient,  $\delta \boldsymbol{\varepsilon}_{pn}$  is the overlap,  $\delta \mathbf{u}_{pn}$  and  $\delta \mathbf{u}_{pt}$  are the relative normal and tangential velocities, and  $\mu_c$  represents the inter-particle friction coefficient, respectively. In above equations,  $r$  is the restitution coefficient, and  $Y^*$ ,  $R^*$ ,  $G^*$  and  $m^*$  are the equivalent Young's modulus, radius, shear modulus and mass, respectively, calculated as follow:

$$\frac{1}{Y^*} = \frac{(1-\nu_1^2)}{Y_1} + \frac{(1-\nu_2^2)}{Y_2}, \quad (9)$$

$$\frac{1}{G^*} = \frac{2(2-\nu_1)(1+\nu_1)}{Y_1} + \frac{2(2-\nu_2)(1+\nu_2)}{Y_2}, \quad (10)$$

$$\frac{1}{R^*} = \frac{1}{R_1} + \frac{1}{R_2}, \quad (11)$$

$$\frac{1}{m^*} = \frac{1}{m_1} + \frac{1}{m_2}, \quad (12)$$

where subscripts 1 and 2 refer to the two particles in contact and  $\nu$  is the Poisson's ratio of the particle. The properties of DEM model is fully presented in Table 1:

Table 1: Material and numerical setup properties

Property	Value	Property	Value
Shear velocity	600 $\mu\text{m/s}$	Sample size	11*1.5*0.8 mm
Particle density	2900 $\text{kg/m}^3$	Particle diameter	90-150 $\mu\text{m}$
DEM time step	$15 \times 10^{-9}$ s	Number of particles	8000
Confining stress	10 MPa	Particle-plate friction	0.9
Particle Poisson ratio	0.25	Particle-particle friction	0.4
Particle restitution coefficient	0.87	Particle Young's modulus	65 GPa

## 2 Gradient Boosting

Gradient boosted trees is an ensemble method for decision trees. We begin this overview with a brief introduction to regression trees [Breiman, 1984; Lundberg et al., 2018], which are the ‘weak learners’ that are iteratively ensembled in this paper. Decision trees are sequentially grown by creating nodes, or ‘decisions’ which partition the data in the most efficient manner. In this case, ‘efficiency’ is accomplished by performing splits in the data which result in maximally dissimilar subsets with respect to the target label (in this case, the macroscopic friction of the simulated system).

The criterion utilized for deciding these splits is the maximum reduction in empirical variance between the two subsets of data partitioned by the split and the data available at the current node. Let  $j$  denote the current node of the tree,  $S_j$  the labels of the subset of data available at the node and  $N_j$  the number of instances in this subset. We also define  $N_{j,L}$  and  $N_{j,R}$  the number of points in the left and right subsets  $S_{j,L}$  and  $S_{j,R}$  respectively resulting from the split, the variance reduction of the node,  $\Delta\text{Var}(S_j)$  can be defined as:

$$\Delta\text{Var}(j) = \text{Var}(S_j) - \frac{N_{j,L}}{N_j} \text{Var}(S_{j,L}) - \frac{N_{j,R}}{N_j} \text{Var}(S_{j,R}) \quad (13)$$

Intuitively, this criterion can be explained in terms of encouraging the within-split group labels to be as similar as possible whilst enforcing the between-split group labels to be as heterogeneous as possible.

The splitting of the data at each node generates two new branches. This process is repeated recursively, generating the decision tree, until a limit is reached (typically the number of data points per node reaches a minimum value, or the tree reaches a maximum depth set by the user), at which point a leaf node is created. When evaluation on the testing set is initiated, each testing instance follows a path through the tree based on the decisions into a leaf node, where it is assigned the average label value in that leaf.

Gradient boosted trees are an ensemble method which builds the aforementioned decision trees sequentially, such that the model improves at each iteration [J. H. Friedman, 2002]. Each subsequent decision tree is fitted to the residuals from the previous iteration. The relationship driving each subsequent model  $\mathbf{h}_t$  and the composite model built so far  $\mathbf{H}_{t-1}$  for a given iteration  $t$  is given by:

$$\mathbf{h}_t, \alpha_t = \text{argmin}(L(\mathbf{y}, \mathbf{H}_{t-1} + \alpha_t \mathbf{h}_t)) + \Omega \mathbf{h}_t \quad (14)$$

$$\mathbf{H}_t = \mathbf{H}_{t-1} + \alpha_t \mathbf{h}_t \quad (15)$$

where  $\mathbf{y}$  is the target label of the regression,  $\alpha_t$  is a scaling constant known as the learning rate,  $L(\dots)$  is the loss function (L2 loss, or square loss in this case), and  $\Omega$  a regularization parameter which punishes the complexity of the model  $\mathbf{h}_t$ .

The gradient boosted trees model shown in this paper takes the features derived from a sliding time window over the pseudo-acoustic emission from a single particle and outputs the a prediction on the macroscopic friction of the system. This model is blind tested on new data not incorporated in the training process: according to which leaves of the model the never seen statistical features fall into, the model outputs an estimate for the macroscopic friction target, without ever having actually seen this data. The performance of this model is shown in Figure 1(c). We used the XGBoost implementation of gradient boosted trees to perform the modelling described in this paper, which enables parallel and distributed computation of the ensemble model ( despite it being sequentially built), and exploits out-of-core computation to enable rapid model exploration for large datasets [Chen & Guestrin, 2016]. This allowed us to quickly explore various feature generation parameters for all 7996 particles in the DEM simulation.

### 3 Model Interpretation

#### 3.1 SHAP values

Within the context of research in the physical sciences, understanding why a machine learning model makes a given prediction can be considered as important, if not more, than the prediction's accuracy. Despite this, the highest accuracy for modern datasets is often accomplished by highly complex 'black-box' models which are extremely difficult to interpret.

For such complex models, we must use a simplified explanation model, which can be defined as an approximation of the original model which is interpretable. To this end, many additive feature attribution methods have recently been developed such as LIME [Ribeiro et al., 2016] or DeepLIFT [Shrikumar et al., 2017]. These explanation models are linear functions of binary variables such that:

$$\mathbf{g}(\mathbf{z}') = \boldsymbol{\varphi}_0 + \sum_{i=1}^M \boldsymbol{\varphi}_i \mathbf{z}'_i \quad (16)$$

Where  $\mathbf{g}(\mathbf{z}')$  is the explanation model, and  $\mathbf{z}' \in (\mathbf{0}, \mathbf{1})^M$  where M is the number of simplified input features and  $\boldsymbol{\varphi}_i$  is the effect of the feature.

These methods satisfy three desirable properties for feature importance attribution:

##### 3.1.1 Local accuracy

The explanation model  $\mathbf{g}(\mathbf{x}')$  should match the original model  $\mathbf{f}(\mathbf{x})$  such that:

$$\mathbf{f}(\mathbf{x}) = \mathbf{g}(\mathbf{x}') = \boldsymbol{\varphi}_0 + \sum_{i=1}^M \boldsymbol{\varphi}_i \mathbf{x}'_i \quad (17)$$

Where  $\mathbf{x}'$  is a simplified input used by the explanation model that maps to the original input through the mapping function  $\mathbf{x} = \mathbf{h}_x(\mathbf{x}')$ . Local accuracy essentially states that the sum of the feature attributions should be equal to the output of the function we are attempting to explain [S. M. Lundberg & Su-In Lee, 2017].

### 3.1.2 Missingness

Missingness is the requirement that features where the simplified input  $\mathbf{x}'_i = \mathbf{0}$  (i.e are missing) should have no attributed impact such that:

$$\mathbf{x}'_i = \mathbf{0} \Rightarrow \varphi_i = \mathbf{0} \quad (18)$$

### 3.1.3 Consistency

Consistency states that modifying a model such that a given feature will have a larger impact on the model can not decrease the importance attribution assigned to said feature.

If:

$$f'_x(\mathbf{z}') - f'_x(\mathbf{z}' \setminus i) \geq f_x(\mathbf{z}') - f_x(\mathbf{z}' \setminus i) \quad (19)$$

For all inputs  $\mathbf{z}' \in (\mathbf{0}, \mathbf{1})^M$ , then:

$$\varphi_i(f', \mathbf{x}) \geq \varphi_i(f, \mathbf{x}) \quad (20)$$

Where  $f'$  is the modified function, and  $f$  is the original function.

Lundberg and Lee demonstrated that the only explanation model that satisfies all three properties, whilst also remaining an additive feature attribution model can be derived from cooperative game theory results [S. M. Lundberg & Su-In Lee, 2017] where feature attributions are interpreted as Shapley values [Shapley, 1953]. In order to define feature attributions in this context, the authors introduced the SHAP value (SHapley Additive ExPlanations), which are Shapley values of a conditional expectation of the model we are trying to explain [S. M. Lundberg & Su-In Lee, 2017]:

$$f_x(\mathbf{S}) = f(\mathbf{h}_x(\mathbf{z}')) = E[f(\mathbf{x}) | \mathbf{x}_S] \quad (21)$$

Where  $\mathbf{S}$  is the set of non-zero indices in  $\mathbf{z}'$ , and  $E[f(\mathbf{x}) | \mathbf{x}_S]$  is the expected value of the function given the subset  $\mathbf{S}$  of the input features [Lundberg et al., 2018]. This conditional expectation is utilized to handle missing values of  $\mathbf{x}_S$  for features not in subset  $\mathbf{S}$ , since models cannot handle arbitrarily selected missing input values [S. M. Lundberg & Su-In Lee, 2017]. By combining this conditional dependence which is used to measure missingness, and the classic Shapley values from cooperative game theory, the following equation defines the SHAP value of a given feature:

$$\varphi_i(f, \mathbf{x}) = \sum_{\mathbf{S} \subseteq \mathbf{N}(i)} \frac{|\mathbf{S}|!(M-|\mathbf{S}|-1)!}{M!} [f_x(\mathbf{S} \cup (i)) - f_x(\mathbf{S})] \quad (22)$$

where  $\mathbf{N}$  represents the entire set of input features, and the sum extends over all subsets  $\mathbf{S}$  of  $\mathbf{N}$  not containing the feature ( $i$ ). This value can be understood as follows: if we imagine the subset of features  $\mathbf{S}$  as a coalition of players playing a game where the aim is to achieve a prediction, then the overall contribution of player ( $i$ ) is calculated by forming the coalition one player at a time over all possible permutations, and averaging over all values of  $f_x(\mathbf{S} \cup (i)) - f_x(\mathbf{S})$ , which is the contribution of the player when they entered the game.

This is a key feature of the SHAP value: game theory demonstrates this is the only possible consistent approach which takes into account all possible orderings of the features, in contrast to

other commonly used feature attribution methods for decision trees such as gain or split count which only take into account a single ordering [Lundberg et al., 2018].

## References

- Anderson, D. L. (2007). *New theory of the Earth*: Cambridge University Press.
- Arce, G. R. (2005). *Nonlinear signal processing: a statistical approach*: John Wiley & Sons.
- Auret, L., & Aldrich, C. (2011). Empirical comparison of tree ensemble variable importance measures. *Chemometrics and Intelligent Laboratory Systems*, 105(2), 157-170. doi:<https://doi.org/10.1016/j.chemolab.2010.12.004>
- Ben-Zion, Y. (2008). Collective behavior of earthquakes and faults: Continuum-discrete transitions, progressive evolutionary changes, and different dynamic regimes. *Rev. Geophys.*, 46(4). doi:doi:10.1029/2008RG000260
- Brace, W. F., & Byerlee, J. D. (1966). Stick-slip as a mechanism for earthquakes. *Science*, 153(3739), 990-992. doi:10.1126/science.153.3739.990
- Brace, W. F., & Byerlee, J. D. (1970). California Earthquakes: Why Only Shallow Focus? *Science*, 168(3939), 1573-1575. doi:10.1126/science.168.3939.1573
- Breiman, L. (1984). *Classification and regression trees*: Routledge.
- Brzinski, T. A., & Daniels, K. E. (2018). Sounds of Failure: Passive Acoustic Measurements of Excited Vibrational Modes. *Physical Review Letters*, 120(21), 218003. doi:10.1103/PhysRevLett.120.218003
- Chen, T., & Guestrin, C. (2016). *XGBoost: A Scalable Tree Boosting System*. Paper presented at the Proceedings of the 22nd ACM SIGKDD International Conference on Knowledge Discovery and Data Mining, San Francisco, California, USA.
- Corbi, F., Sandri, L., Bedford, J., Funicello, F., Brizzi, S., Rosenau, M., & Lallemand, S. (2019). Machine Learning can predict the timing and size of analog earthquakes. *Geophysical Research Letters*. doi:doi:10.1029/2018GL081251
- Dahmen, K. A., Ben-Zion, Y., & Uhl, J. T. (2011). A simple analytic theory for the statistics of avalanches in sheared granular materials. *Nature Physics*, 7, 554. doi:10.1038/nphys1957  
<https://www.nature.com/articles/nphys1957#supplementary-information>
- Di Renzo, A., & Di Maio, F. P. (2004). Comparison of contact-force models for the simulation of collisions in DEM-based granular flow codes. *Chemical Engineering Science*, 59(3), 525-541. doi:10.1016/j.ces.2003.09.037
- Đorić, D., Nikolić-Đorić, E., Jevremović, V., & Mališić, J. J. Q. (2009). On measuring skewness and kurtosis. *Quality and Quantity*, 43(3), 481-493. doi:10.1007/s11135-007-9128-9
- Dorostkar, O. (2018). *Stick-slip dynamics in dry and fluid saturated granular fault gouge investigated by numerical simulations*. (PhD Dissertaion ), ETH Zurich,

- Dorostkar, O., & Carmeliet, J. (2018). Potential Energy as Metric for Understanding Stick–Slip Dynamics in Sheared Granular Fault Gouge: A Coupled CFD–DEM Study. *Rock Mechanics and Rock Engineering*. doi:10.1007/s00603-018-1457-6
- Dorostkar, O., & Carmeliet, J. (2019). Grain Friction Controls Characteristics of Seismic Cycle in Rough Faults with Granular Gouge *EarthArXiv*. doi:doi:10.31223/osf.io/64jx2
- Dorostkar, O., Guyer, R. A., Johnson, P. A., Marone, C., & Carmeliet, J. (2017). On the micromechanics of slip events in sheared, fluid saturated fault gouge. *Geophysical Research Letters*, 6101–6108. doi:10.1002/2017GL073768
- Dorostkar, O., Guyer, R. A., Johnson, P. A., Marone, C., & Carmeliet, J. (2018). Cohesion-induced stabilization in stick-slip dynamics of weakly wet, sheared granular fault gouge. *Journal of Geophysical Research: Solid Earth*. doi:10.1002/2017JB015171
- Dorostkar, O., Johnson, P., Guyer, R., Marone, C., & Carmeliet, J. (2017). Do Fluids Modify the Stick-Slip Behavior of Sheared Granular Media? *Poromechanics VI : Proceedings of the Sixth Biot Conference on Poromechanics, 2017*. , 158-163. doi:10.1061/9780784480779.019
- Friedman, J., Hastie, T., & Tibshirani, R. (2000). Additive logistic regression: a statistical view of boosting (with discussion and a rejoinder by the authors). *The Annals of Statistics*, 28(2), 337-407.
- Friedman, J. H. (2002). Stochastic gradient boosting. *Computational Statistics*, 38(4), 367-378.
- Goniva, C., Kloss, C., Deen, N. G., Kuipers, J. A. M., & Pirker, S. (2012). Influence of rolling friction on single spout fluidized bed simulation. *Particuology*, 10(5), 582-591. doi:10.1016/j.partic.2012.05.002
- Greenwell, B. M. (2017). pdp: An R Package for Constructing Partial Dependence Plots. *R Journal*, 9(1).
- Gutenberg, B., & Richter, C. F. (1944). Frequency of earthquakes in California\*. *Bulletin of the Seismological Society of America*, 34(4), 185-188.
- Hertz, H. (1882). Ueber die Berührung fester elastischer Körper. *Journal für die reine und angewandte Mathematik*, 92, 156-171.
- Hulbert, C., Rouet-Leduc, B., Johnson, P. A., Ren, C. X., Rivière, J., Bolton, D. C., & Marone, C. (2019). Similarity of fast and slow earthquakes illuminated by machine learning. *Nature Geoscience*, 12(1), 69-74. doi:10.1038/s41561-018-0272-8
- Johnson, T., Wu, F. T., & Scholz, C. H. (1973). Source parameters for stick-slip and for earthquakes. *Science*, 179(4070), 278-280. doi:10.1126/science.179.4070.278
- Kloss, C., Goniva, C., Hager, A., Amberger, S., & Pirker, S. (2012). Models, algorithms and validation for opensource DEM and CFD-DEM. *Progress in Computational Fluid Dynamics*, 12(2-3), 140-152.

- Kong, Q., Trugman, D. T., Ross, Z. E., Bianco, M. J., Meade, B. J., & Gerstoft, P. (2018). Machine Learning in Seismology: Turning Data into Insights. *Seismological Research Letters*, 90(1), 3-14. doi:10.1785/0220180259
- Lundberg, S. M., Erion, G. G., & Lee, S.-I. (2018). Consistent Individualized Feature Attribution for Tree Ensembles. *arXiv preprint arXiv:1803.03888*.
- Lundberg, S. M., & Lee, S.-I. (2017). Consistent feature attribution for tree ensembles. *arXiv preprint arXiv:1706.06060*.
- Lundberg, S. M., & Lee, S.-I. (2017). *A unified approach to interpreting model predictions*. Paper presented at the Advances in Neural Information Processing Systems.
- McBrearty, I. W., Delorey, A. A., & Johnson, P. A. (2019). Pairwise Association of Seismic Arrivals with Convolutional Neural Networks. *Seismological Research Letters*.
- Meroz, Y., & Meade, B. J. (2017). Intermittent Granular Dynamics at a Seismogenic Plate Boundary. *Physical Review Letters*, 119(13), 138501. doi:10.1103/PhysRevLett.119.138501
- MiDi, G. D. R. (2004). On dense granular flows. *European Physical Journal E*, 14(4), 341-365. doi:10.1140/epje/i2003-10153-0
- Perol, T., Gharbi, M., & Denolle, M. (2018). Convolutional neural network for earthquake detection and location. *SCIENCE ADVANCES*, 4(2), e1700578. doi:10.1126/sciadv.1700578 %J Science Advances
- Ribeiro, M. T., Singh, S., & Guestrin, C. (2016). *Why should i trust you?: Explaining the predictions of any classifier*. Paper presented at the Proceedings of the 22nd ACM SIGKDD international conference on knowledge discovery and data mining.
- Rivière, J., Lv, Z., Johnson, P. A., & Marone, C. (2018). Evolution of b-value during the seismic cycle: Insights from laboratory experiments on simulated faults. *Earth and Planetary Science Letters*, 482, 407-413. doi:<https://doi.org/10.1016/j.epsl.2017.11.036>
- Ross, Z. E., Meier, M. A., Hauksson, E., & Heaton, T. H. (2018). Generalized seismic phase detection with deep learning. *Bulletin of the Seismological Society of America*, 108(5A), 2894-2901.
- Ross, Z. E., Yue, Y., Meier, M.-A., Hauksson, E., & Heaton, T. H. (2019). PhaseLink: A Deep Learning Approach to Seismic Phase Association. *Journal of Geophysical Research: Solid Earth*, 0(ja). doi:doi:10.1029/2018JB016674
- Rouet-Leduc, B., Hulbert, C., Bolton, D. C., Ren, C. X., Riviere, J., Marone, C., . . . Johnson, P. A. (2018). Estimating Fault Friction From Seismic Signals in the Laboratory. *Geophysical Research Letters*. doi:10.1002/2017GL076708

- Rouet-Leduc, B., Hulbert, C., & Johnson, P. A. (2019). Continuous chatter of the Cascadia subduction zone revealed by machine learning. *Nature Geoscience*, *12*(1), 75-79. doi:10.1038/s41561-018-0274-6
- Rouet-Leduc, B., Hulbert, C., Lubbers, N., Barros, K., Humphreys, C. J., & Johnson, P. A. (2017). Machine Learning Predicts Laboratory Earthquakes. *Geophysical Research Letters*, *44*(18), 9276-9282. doi:10.1002/2017GL074677
- Scholz, C. H. (1998). Earthquakes and friction laws. *Nature*, *391*(6662), 37-42. doi:10.1038/34097
- Shapley, L. S. (1953). A value for n-person games. *Contributions to the Theory of Games*, *2*(28), 307-317.
- Shrikumar, A., Greenside, P., & Kundaje, A. (2017). Learning important features through propagating activation differences. *arXiv preprint arXiv:1704.00027*.
- Uhl, J. T., Pathak, S., Schorlemmer, D., Liu, X., Swindeman, R., Brinkman, B. A. W., . . . Dahmen, K. A. (2015). Universal Quake Statistics: From Compressed Nanocrystals to Earthquakes. *Scientific Reports*, *5*, 16493. doi:10.1038/srep16493
- <https://www.nature.com/articles/srep16493#supplementary-information>
- van der Elst, N. J., Brodsky, E. E., Le Bas, P.-Y., & Johnson, P. A. (2012). Auto-acoustic compaction in steady shear flows: Experimental evidence for suppression of shear dilatancy by internal acoustic vibration. *Journal of Geophysical Research: Solid Earth*, *117*(B9). doi:10.1029/2011JB008897